scientific reports

Check for updates

OPEN

Significance of nanoparticles aggregation on the dynamics of rotating nanofluid subject to gyrotactic microorganisms, and Lorentz force

Bagh Ali[1,2], Imran Siddique[3]✉, Rifaqat Ali[4], Jan Awrejcewicze[5], Fahd Jarad[6,7]✉ & Hamiden Abd El-Wahed Khalifa[8,9]✉

The significance of nanoparticle aggregation, Lorentz and Coriolis forces on the dynamics of spinning silver nanofluid flow past a continuously stretched surface is prime significance in modern technology, material sciences, electronics, and heat exchangers. To improve nanoparticles stability, the gyrotactic microorganisms is consider to maintain the stability and avoid possible sedimentation. The goal of this report is to propose a model of nanoparticles aggregation characteristics, which is responsible to effectively state the nanofluid viscosity and thermal conductivity. The implementation of the similarity transforQ1m to a mathematical model relying on normal conservation principles yields a related set of partial differential equations. A well-known computational scheme the FEM is employed to resolve the partial equations implemented in MATLAB. It is seen that when the effect of nanoparticles aggregation is considered, the temperature distribution is enhanced because of aggregation, but the magnitude of velocities is lower. Thus, showing the significance impact of aggregates as well as demonstrating themselves as helpful theoretical tool in future bioengineering and industrial applications.

Nanofluids are made by suspending nanoparticles in a liquid carrier such as oil, argon, or ethylene glycol[1]. The presence of nanomaterials in the host fluid has a significant impact on the thermophysical features of base fluids with low conductivity properties, according to theoretical and experimental findings[2–4]. Due to their interesting uses in every aspect of science and engineering, the convective nanofluid thermal transport flow attention a large number of researchers. To mention several, the ceramic nanomaterials and diamond are utilized to improve the mineral-oil dielectric properties, the liquid incorporated nanomaterials can be utilized for directly sunlight absorption in solar collectors, making them suitable for biomedical uses including cancer therapy and drug delivery etc.[5–7]. The several numerically computational have been studied to enhance the fluid thermal conductivity like, peristaltic pumping of a nanofluid[8], Casson fluid incorporated nanoparticles[9], magnetized nanoparticles subject to water as a host fluid[10], hybrid nanoparticles considered to enhance the performance of DC operated micropump[11], non-uniform heat source/sink with nanoparticles incorporated in the base fluid to observe the heat transfer rate[12], thermal enhancement through multi-twisted tape subject to tiny particles[13], and hydrothermal nanofluid analysis subject to wavy pipe geometry[14].

[1]School of Mathematics and Statistics, Northwestern Polytechnical University, Xi'an 710129, China. [2]Faculty of Sciences, Superior University, Lahore 54000, Pakistan. [3]Department of Mathematics, University of Management and Technology, Lahore 54770, Pakistan. [4]Department of Mathematics, College of Science and Arts, King Khalid University, Muhayil, Abha 61413, Saudi Arabia. [5]Department of Automation, Biomechanics and Mechatronics, Lodz University of Technology, 1/15 Stefanowskiego St., 90 924 Lodz, Poland. [6]Department of Mathematics, Cankaya University, Etimesgut, Ankara, Turkey. [7]Department of Medical Research, China Medical University Hospital, China Medical University, Taichung, Taiwan. [8]Department of Mathematics, College of Sciences and Arts, Qassim University, Al-Badaya 51951, Saudi Arabia. [9]Department of Operations Research, Faculty of Graduate Studies for Statistical Research, Cairo University, Giza 12613, Egypt. ✉email: imransmsrazi@gmail.com; fahd@cankaya.edu.tr; hamiden@cu.edu.eg

The rotatory flow has wide range of applications in real life, such as turbine rotors, air cleaner devices, mixing materials machinery, medical field, and power generation systems, etc.[15,16]. The first endeavor towards the rotating path of fluid was made by Wang[17]. Many researchers are investigated the rotating flow under different aspects and geometries are given in Refs.[18–21]. The presence of a density gradient in the flow field causes the bio convective phenomenon. Consequently, the movement of the particles at the macroscopic level causes the improvement of the density stratification of the base liquid in one direction. Many researchers were interested in the existence of such Gyrotactic microorganisms in the nanofluid flow because of their potential applications in enzymes, biotechnology, biosensors, biofuels, and medication delivery. These applications prompted a number of investigators to do numerical simulations on bio convective nanofluid flow with microorganisms passing through a variety of flow fields. Chu et al.[22] have used Homotopy Analysis Approach to evaluate numerically bio convection Maxwell nanofluid flow via bidirectional periodically moving plate under nonlinear radiation and heat source phenomena. Rao et al.[23] scrutinized the bio convective flow in a conventional reactive nanofluid towards the isothermal upright cone with Gyrotactic microorganisms immersed in a permeable medium. Awais et al.[24] investigated assisting and opposing bio convective nanofluid flow with motile microorganisms numerically via Adams–Bash forth approach (ABA). Abdelmalek et al.[25] investigated bio-convective third-grade nanofluid stream over an extending sheet under Arrhenius activation energy by using bvp4c. Shafiq et al.[26] investigated the chemically reactant bio-convective second grade nanofluid flow under buoyancy effect.

Numerous investigators came to the conclusion that particle aggregation[27,28], particle motion[29] and liquid-layering[30] are most valuable variables in thermal conductivity processes in nanofluids. The fact that particle aggregation can improve nanofluids' efficient thermal conductivity has been demonstrated experimentally[30,31]. According to Wang et al.[32], particle clustering could have a noteworthy effect on the improvement of thermal conductivity of nanoliquid. In[33], authors proposed a mixture model to describe two-component heterogeneous structures. The particle aggregation form is invariable in their model that ignores the impact of aggregation shape on nanofluids effective thermal conductivity.

The extensive literature review stated above reveals that the minimal attention to the self-motile thermophile microorganisms ingrained nanofluid rotating flow across a stretching sheet with the impact of the external magnetic field subject to nanoparticles aggregation. According to the author's insight, none of the listed articles discuss the detailed problem. The main objective of this study is to examine the heat and mass transport impacts of transitory hydromagnetic rotating nanofluid three-dimensional flows with Gyrotactic microbes. Numerous scholars have lately examined the hydromagnetics nanofluid flow for Newtonian and non-Newtonian flow[34–36] by utilizing variational finite element technique. The coupled non-linear PDEs is resolved using a control volume technique with a weighted residual approach using a Galerkin FEM[37,38]. The flow field characteristics for a variety of important parameter modifications are explored and illustrated graphically. The MATLAB code blocks yielded computational findings that were validated by existing literature and determined to have a reasonable correlation. This numerical analysis applies to gasoline, polymers, nutrition release precision, engine lubricants, paint rheology, Bio-Sensors, medicine delivery, and biofuels.

Research questions. The following relevant scientific research questions are examined in the study:

1. To explore the impact of Coriolis force and Lorentz force on thermal, momentum, and concentration profiles in the presence and absence of nanoparticle aggregation?
2. What impact do the Coriolis and Lorentz forces have on mass transport rate, skin friction factor, and thermal efficiency presence and absence of nanoparticle aggregation?
3. What are the impacts of Brownian motion, thermophoresis, and time-dependent parameters on thermal distribution?
4. Evaluate how bio-convection affects the microorganisms profile in the presence and absence of nanoparticle aggregation?

Mathematical formulation

Consider a MHD three-dimensional rotating Maxwell nanofluid flow across a bidirectional stretching surface. Figure 1 depicts the fluid dynamic structure and three-dimensional the developed problem. The flow is limited to $z \geq 0$. The fixed origin $O(x, y, z)$ has been chosen, with the *x-axis* depicting the stretching surface's movement, the y axis depicting the surface's normal, and the *z-axis* depicting transverse to the *xy* plane. A static and uniform magnetic $B0$ field is applied in the axial direction (z-direction). Due to the low magnetic Reynolds number, a reduced magnetic field is created, hence Ohmic dissipation and Hall current are negligible[39]. T_∞, N_w, C_∞, represents ambient temperature and concentration and T_w, N_w, C_w, signifies surface temperature and concentration. To avoid sedimentation, gyrotactic microorganisms is taken into account to maintain convection stability. $V = (u_1(x, y, z), u_2(x, y, z), u_3(x, y, z))$ considers the velocity field in the current complicated situation. The physical properties of nanoparticles aggregation and without aggregation, and based fluid are mentioned in the Tables 1 and 2. The governing equations of continuity, momentum, temperature, concentration and bioconvection of the fluid flow are given as[40–42]:

$$u_{1x} + u_{2y} + u_{3z} = 0, \tag{1}$$

$$\rho_{nf}(u_{1t} + u_1 u_{1x} + u_2 u_{1y} + u_3 u_{1z} + 2\Omega u_2) = \mu_{nf} u_{1zz} - \sigma_{nf} B_0^2 u_1, \tag{2}$$

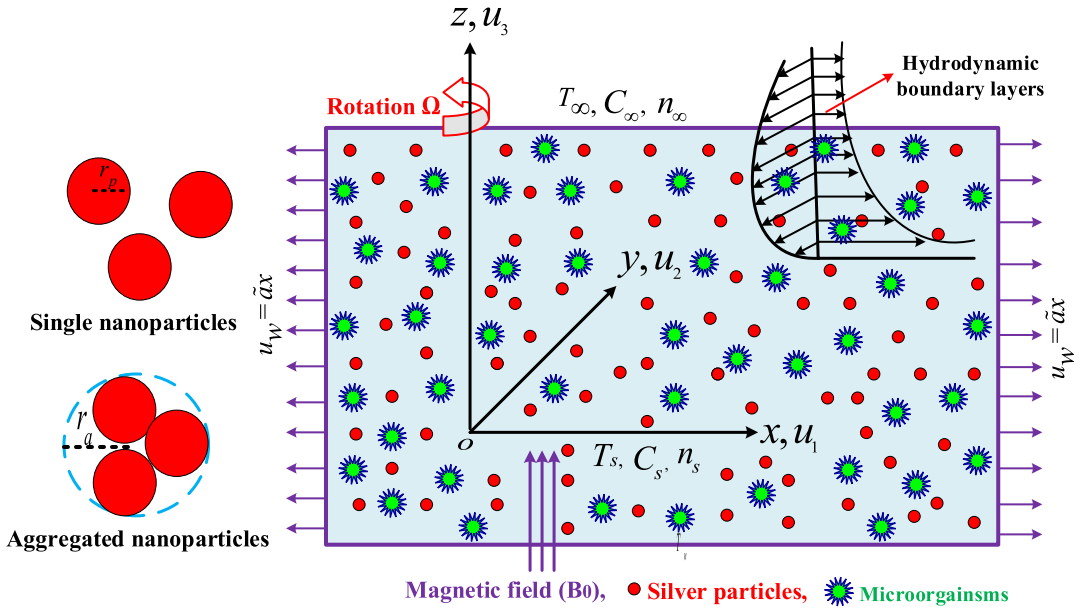

Figure 1. Physical representation of problem.

Physical properties	ρ (kg m^{-3})	C_p (J/kg K)	κ (W/m K)
H_2O	0991.1	4179.0	00.613
TiO_2	4250.0	686.20	8.9538

Table 1. Thermo-physical properties of water base fluid and nanoparticles[45].

Properties	With aggregation	Without aggregation
viscosity (μ)	$\frac{\mu_{n_f}}{\mu_f} = (1 - \frac{\Phi_{ag}}{\Phi_m})^{2.5\Phi_m}$	$\frac{\mu_{n_f}}{\mu_f} = \frac{1}{(1-\Phi)^{2.5}}$
density (ρ)	$\rho_{n_f} = \rho_f(1 - \Phi_{ag}) + \Phi_{ag}\rho_s$	$\rho_{n_f} = \rho_f(1 - \Phi) + \Phi\rho_s$
Heat capacity(ρC_p)	$(\rho C_p)_{nf} = (\rho C_p)_f(1 - \Phi_{ag}) + \Phi_{ag}\frac{(\rho C_p)_s}{(\rho C_p)_f}$	$(\rho C_p)_{nf} = (\rho C_p)_f(1 - \Phi) + \Phi\frac{(\rho C_p)_s}{(\rho C_p)_f}$
Thermal conductivity(κ)	$\frac{k_{n_f}}{k_f} = \frac{k_{ag}+2k_f-2\Phi_{ag}(k_f-k_{ag})}{k_{ag}+2k_f+\Phi_{ag}(k_f-k_{ag})}$	$\frac{k_{n_f}}{k_f} = \frac{k_s+2k_f-2\Phi(k_f-k_s)}{k_s+2k_f+\Phi(k_f-k_s)}$

Table 2. Thermo-physical attributes of base fluid and nanoparticles[45,46].

$$\rho_{nf}(u_{2t} + u_1u_{2x} + u_2u_{2y} + u_3u_{2z} - 2\Omega u_1) = \mu_{nf}u_{2zz} - \sigma_{n_f}B_0^2u_2, \tag{3}$$

$$T_t + u_1T_x + u_2T_y + u_3T_z = \alpha_{n_f}T_{zz} + \tau^*\{D_bC_zT_z + \frac{D_T}{T_\infty}T_z^2\}, \tag{4}$$

$$C_t + u_1C_x + u_2C_y + u_3C_z = D_bC_{zz} + \frac{D_T}{T_\infty}T_{zz}, \tag{5}$$

$$n_t + u_1n_x + u_2n_y + u_3n_z + \frac{bWc}{(C_s - C_\infty)}[(nC_z)_z] = D_mN_{zz}, \tag{6}$$

where $\rho_{nf}, \mu_{n_f}, \alpha_{n_f}$, are the fluid density, dynamic viscosity and thermal diffusivity, C indicates the nanoparticles concentration, n symbolizes microorganisms concentration, T represnts the fluid temperature, D_T, D_N, and D_B, are represents the thermophoretic diffusion coefficient, diffusivity of microorganisms, and Brownian diffusion coefficients, respectively. The boundary constraints are[43,44]:

$$t < 0 : u_1 = 0,\ u_2 = 0,\ u_3 = 0,\ C = C_\infty,\ T = T_\infty,\ n = n_\infty, \tag{7}$$

$$t \geq 0 : u_1 = \tilde{a}x,\ u_3 = u_2 = 0,\ T = T_s,\ C = C_s,\ n = n_s,\ as\ z = 0, \tag{8}$$

$$t \geq 0 : u_1 \to 0,\ u_2 \to 0,\ T \to T_\infty,\ C \to C_\infty,\ n \to n_\infty,\ as\ z \to \infty. \tag{9}$$

Similarity transformations (see[40,43]):

$$\left.\begin{aligned} u_1 = \tilde{a}x\frac{\partial F_1(\Gamma,\eta)}{\partial \eta},\ u_2 = \tilde{a}xF_2(\Gamma,\eta),\ u_3 = -\sqrt{\tilde{a}\nu}\Gamma F_1(\Gamma,\eta),\ \ \Gamma = 1-e^{-\zeta}, \eta = \sqrt{\frac{\tilde{a}xz^2}{\Gamma\nu}},\\ \zeta = \tilde{a}t,\ \frac{T-T_\infty}{(T_s-T_\infty)} = \Theta(\Gamma,\eta),\ \frac{C-C_\infty}{(C_s-C_\infty)} = \Phi(\Gamma,\eta),\ \frac{n-n_\infty}{(n_s-n_\infty)} = \chi(\Gamma,\eta). \end{aligned}\right\} \tag{10}$$

In view of Eq. (10), Eq. (1) is satisfied and Eqs. (2–9) becomes non-linear PDEs into transformed coordinate systems (Γ, η).

$$\frac{1}{\chi_1\chi_2}F_1''' + 0.5\eta F_1'' - 0.5\Gamma\eta F_1'' + \Gamma(F_1F_1'' - F_1'^2 - \frac{M^2}{\chi_2}F_1' + 2\lambda F_2) - \Gamma(1-\Gamma)\frac{\partial F_1'}{\partial \Gamma} = 0, \tag{11}$$

$$\frac{1}{\chi_1\chi_2}F_2'' + 0.5\eta F_2' - 0.5\Gamma\eta F_2' + \Gamma(F_1F_2' - 2\lambda F_1' - \frac{M^2}{\chi_2}F_2 - F_1'F_2) - \Gamma(1-\Gamma)\frac{\partial F_2}{\partial \Gamma} = 0, \tag{12}$$

$$\frac{\chi_3}{\chi_4}\Theta'' + 0.5\eta(1-\Gamma)P_r\Theta' + \Gamma P_rF_1\Theta' + N_bP_r\Theta\Phi + N_tP_r\Theta'^2 - \Gamma(1-\Gamma)P_r\frac{\partial\Theta}{\partial\Gamma} = 0, \tag{13}$$

$$\Phi'' + 0.5\eta S_c(1-\Gamma)\Phi' + S_c\Gamma F_1\Phi' + N_tN_b^{-1}\Theta'' - \Gamma(1-\Gamma)S_c\frac{\partial\Phi}{\partial\Gamma} = 0, \tag{14}$$

$$\chi'' + \frac{S_b}{2}(1-\Gamma)S_b\chi' + \Gamma S_bF_1\chi' - P_e\Phi''(\delta_1+\chi) + P_e\chi'\Phi' = S_b\Gamma(1-\Gamma)\frac{\partial\chi}{\partial\Gamma}, \tag{15}$$

$$\left.\begin{aligned} \lim_{\eta\to 0}F_1(\Gamma,\eta) = 0,\ \lim_{\eta\to 0}F_1'(\Gamma,\eta) = 1, \lim_{\eta\to 0}F_2(\Gamma,\eta) = 0, \lim_{\eta\to 0}\Theta(\Gamma,\eta) = \lim_{\eta\to 0}\Phi(\Gamma,\eta) = \lim_{\eta\to 0}\chi(\Gamma,\eta) = 1,\ \Gamma \geq = 0,\\ \lim_{\eta\to\infty}F_1'(\Gamma,\eta) \to 0, \lim_{\eta\to\infty}F_2(\Gamma,\eta) \to 0, \lim_{\eta\to\infty}\Theta(\Gamma,\eta) \to 0, \lim_{\eta\to\infty}\Phi(\Gamma,\eta) \to 0, \lim_{\eta\to\infty}\chi(\Gamma,\eta) \to 0,\ \Gamma \geq 0, \end{aligned}\right\} \tag{16}$$

where

$$\chi_1 = \left(1-\frac{\Phi_{ag}}{\Phi_m}\right)^{-2.5\Phi_m},\ \chi_2 = (1-\Phi_{ag}) + \Phi_{ag}\frac{\rho_{ag}}{\rho_f},\ \chi_3 = \frac{k_{ag}+2k_f-2\Phi_{ag}(k_f-k_{ag})}{k_{ag}+2k_f+\Phi_{ag}(k_f-k_{ag})},$$
$$\chi_4 = (1-\Phi_{ag}) + \Phi_{ag}\frac{(\rho C_p)_{ag}}{(\rho C_p)_f},$$

and $\lambda = \frac{\Omega}{a}$ signifies rotating parameter, $M = \sqrt{\frac{\sigma_{n_f}B_o^2}{\rho_f\tilde{a}}}$ deliberated the magnetic parameter, $P_r = \frac{\nu}{\alpha_{n_f}}$ symbolize the Prandtl number, $S_c = \frac{\nu}{D_b}$ is the Schmidt number $S_b = \frac{\nu}{D_m}$ represent bioconvection Schmidt number , $N_b = \tau\nu^{-1}D_B(C_s - C_\infty)$ is the Brownian motion, $N_t = \frac{D_T(\tau T_s^m \tau T_\infty)}{\nu T_\infty}$ represent the thermophoresis , $P_e = \frac{bW_c}{D_m}$ Peclet number, $\delta_1 = \frac{n_\infty}{n_s - n_\infty}$ is microorganism-concentration difference.

The following are the local skin friction coefficients, Sherwood coefficients, and Nusselt coefficients respectively as follows:

$$Nu = \frac{xq_w}{\kappa(T_s - T_\infty)}, \tag{17}$$

$$Shr = \frac{xq_m}{D_b(C_s - C_\infty)}, \tag{18}$$

$$C_{f_x} = \frac{\tau_w^x}{\rho u_1^2}, \tag{19}$$

$$C_{f_y} = \frac{\tau_w^y}{\rho u_1^2}. \tag{20}$$

Using Eq. (10), we derive the following results:

$$\begin{cases} C_{f_x} Re_x{}^{1/2} = \dfrac{F_1{}''(0)}{\sqrt{\Gamma}}, C_{f_y} Re_x{}^{1/2} = \dfrac{F_2{}'(0)}{\sqrt{\Gamma}}, \\ Nu_x Re_x{}^{1/2} = -\dfrac{[\Theta'(0)]}{\sqrt{\Gamma}}, Shr_x Re_x{}^{1/2} = -\dfrac{[\Phi'(0)]}{\sqrt{\Gamma}}. \end{cases} \tag{21}$$

Numerical procedure

The FEM is renowned for its ability to solve several types of DE. This process utilizes continuous piecewise approximation to reduce the amount of the inaccuracy[47]. The critical phases and a wonderful depiction of this method are laid out by Reddy[48] and jyothi[49]. Because to its precision and computability, experts believe this numerical approach is a particularly effective instrument for solving current engineering and industrial challenges[50,51]. To solve Eq. (11) to (15) together with boundary condition (18), take this into consideration:

$$F_1' = H, \tag{22}$$

Equations (11)–(16) are simplified to a lower order:

$$\frac{1}{\chi_1 \chi_2} H'' + 0.5(1-\Gamma)\eta H' + \Gamma(F_1 H' - H^2 + 2\lambda F_2 - \frac{M^2}{\chi_2} H) = \Gamma(1-\Gamma)\frac{\partial H}{\partial \Gamma}, \tag{23}$$

$$\frac{1}{\chi_1 \chi_2} F_2'' + \frac{1}{2}(1-\Gamma)\eta F_2{}' + \Gamma(F_1 F_2{}' - H F_2 - 2\lambda H - \frac{M^2}{\chi_2} F_2) = \Gamma(1-\Gamma)\frac{\partial F_2}{\partial \Gamma}, \tag{24}$$

$$\frac{\chi_3}{\chi_4}\Theta'' + 0.5\eta(1-\Gamma)P_r\Theta' + P_r\Gamma F_1\Theta' + N_b P_r \Theta'\Phi' + N_t P_r \Theta'^2 = P_r\Gamma(1-\Gamma)\frac{\partial \Theta}{\partial \Gamma}, \tag{25}$$

$$\Phi'' + 0.5 S_c(1-\Gamma)\eta\Phi' + S_c\Gamma F_1\Phi' + N_t N_b^{-1}\Theta''^2 = \Gamma(1-\Gamma)S_c\frac{\partial \Phi}{\partial \Gamma}, \tag{26}$$

$$\chi'' + \frac{S_b}{2}(1-\Gamma)\eta\chi' + \Gamma S_b F_1 \chi' - P_e\Phi''(\delta_1 + \chi) + P_e\chi'\Phi' = S_b\Gamma(1-\Gamma)\frac{\partial \chi}{\partial \Gamma}, \tag{27}$$

$$\left.\begin{aligned} &\lim_{\eta\to 0} F_1(\Gamma,\eta) = 0,\ \lim_{\eta\to 0} H(\Gamma,\eta) = 1,\ \lim_{\eta\to 0} F_2(\Gamma,\eta) = 0,\ \lim_{\eta\to 0}\Theta(\Gamma,\eta) = \lim_{\eta\to 0}\Phi(\Gamma,\eta) = \lim_{\eta\to 0}\chi(\Gamma,\eta) = 1,\ \Gamma \geq = 0, \\ &\lim_{\eta\to\infty} H(\Gamma,\eta) \to 0,\ \lim_{\eta\to\infty} F_2(\Gamma,\eta) \to 0,\ \lim_{\eta\to\infty}\Theta(\Gamma,\eta) \to 0,\ \lim_{\eta\to\infty}\Phi(\Gamma,\eta) \to 0,\ \lim_{\eta\to\infty}\chi(\Gamma,\eta) \to 0,\ \Gamma \geq 0. \end{aligned}\right\} \tag{28}$$

The plate thickness $\eta = 6.0$ and length $\Gamma = 1.0$ are fixed for numerical computations. Equations (22)–(27) have a variational form that may be represented as:

$$\int_{\Omega_e} w_{f_1}\{F_1' - H\} d\Omega_e = 0, \tag{29}$$

$$\int_{\Omega_e} w_{f_2}\left\{\frac{1}{\chi_1\chi_2}H'' + \frac{1}{2}(1-\Gamma)\eta H' + \Gamma(F_1 H' - H^2 + 2\lambda H - M^2 H) - \Gamma(1-\Gamma)\frac{\partial H}{\partial \Gamma}\right\} d\Omega_e = 0, \tag{30}$$

$$\int_{\Omega_e} w_{f_3}\left\{\frac{1}{\chi_1\chi_2}F_2'' + \frac{1}{2}(1-\Gamma)\eta F_2{}' + \Gamma(F_1 F_2{}' - H F_2 - 2\lambda H) - \Gamma(1-\Gamma)\frac{\partial F_2}{\partial \Gamma}\right\} d\Omega_e = 0, \tag{31}$$

$$\int_{\Omega_e} w_{f_4}\left\{\frac{\chi_3}{\chi_4}\Theta'' + \frac{P_r}{2}(1-\Gamma)\eta\Theta' + P_r\Gamma F_1\Theta' + N_b P_r\Theta'\Phi' + N_t P_r(\Theta')^2 - P_r\Gamma(1-\gamma)\frac{\partial \Theta}{\partial \Gamma}\right\} d\Omega_e = 0, \tag{32}$$

$$\int_{\Omega_e} w_{f_5}\left\{\Phi'' + 0.5 S_c\eta(1-\Gamma)\Phi' + \Gamma S_c F_1\Phi' + \frac{N_t}{N_b}(\Theta'')^2 - \Gamma(1-\Gamma)S_c\frac{\partial \Phi}{\partial \Gamma}\right\} d\Omega_e = 0, \tag{33}$$

$$\int_{\Omega_e} w_{f_6}\left\{\chi'' + \frac{S_b}{2}(1-\Gamma)\eta\chi' + \Gamma S_b F_1\chi' - P_e\left(\Phi''(\delta_1 + \chi) + \chi'\Phi'\right) - \Gamma(1-\Gamma)S_b\frac{\partial \chi}{\partial \Gamma}\right\} d\Omega_e = 0. \tag{34}$$

Here $w_{f_s}(s = 1, 2, 3, 4, 5, 6)$ indicates the trial functions. Let divide the input (Ω_e) split into four nodded components (see Fig. 2). The following are finite element estimations:

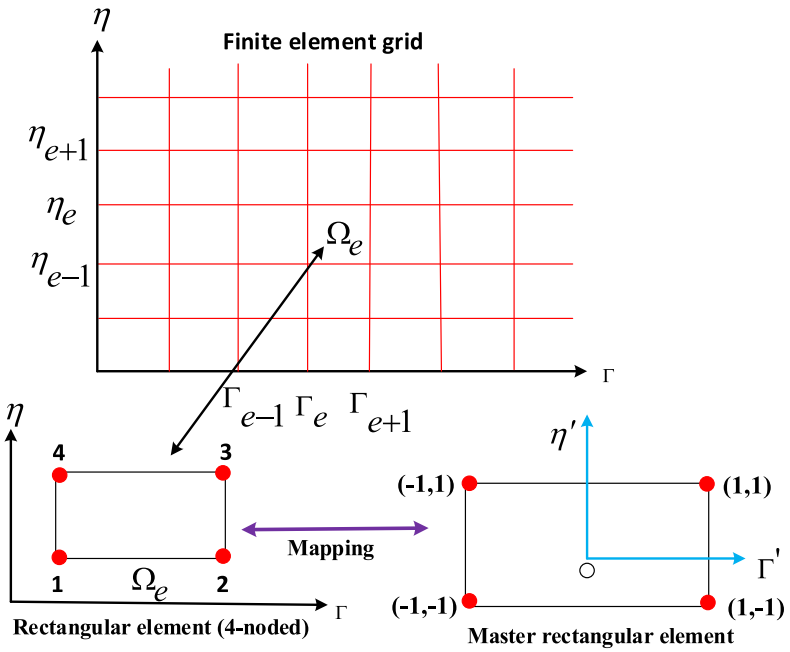

Figure 2. Finite element mesh and grid.

$$F_1 = \sum_{j=1}^{4} F_{1j}\Upsilon_j(\gamma,\eta),\ H = \sum_{j=1}^{4} H_j\Upsilon_j(\Gamma,\eta),\ F_2 = \sum_{j=1}^{4} F_{2j}\Upsilon_j(\Gamma,\eta),\ \Theta = \sum_{j=1}^{4} \Theta_j\Upsilon_j(\Gamma,\eta),\ \Phi = \sum_{j=1}^{4} \Phi_j\Upsilon_j(\Gamma,\eta). \tag{35}$$

Here, Υ_j (j = 1,2,3,4) are the linear interpolation shapes functions for Ω_e as:

$$\left.\begin{aligned} \Upsilon_1 &= \frac{(\Gamma_{e+1}-\Gamma)(\eta_{e+1}-\eta)}{(\Gamma_{e+1}-\Gamma_e)(\eta_{e+1}-\eta_e)},\ \Upsilon_2 = \frac{(\Gamma-\Gamma_e)(\eta_{e+1}-\eta)}{(\Gamma_{e+1}-\Gamma_e)(\eta_{e+1}-\eta_e)},\\ \Upsilon_3 &= \frac{(\Gamma-\Gamma_e)(\eta-\eta_e)}{(\Gamma_{e+1}-\Gamma_e)(\eta_{e+1}-\eta_e)},\ \Upsilon_4 = \frac{(\Gamma_{e+1}-\Gamma)(\eta-\eta_e)}{(\Gamma_{e+1}-\Gamma_e)(\eta_{e+1}-\eta_e)}. \end{aligned}\right\} \tag{36}$$

The following is the developed finite element model of the equations:

$$\begin{bmatrix} [L^{11}] & [L^{12}] & [L^{13}] & [L^{14}] & [L^{15}] & [L^{16}] \\ [L^{21}] & [L^{22}] & [L^{23}] & [L^{24}] & [L^{25}] & [L^{26}] \\ [L^{31}] & [L^{32}] & [L^{33}] & [L^{34}] & [L^{35}] & [L^{36}] \\ [L^{41}] & [L^{42}] & [L^{43}] & [L^{44}] & [L^{45}] & [L^{45}] \\ [L^{51}] & [L^{52}] & [L^{53}] & [L^{54}] & [L^{55}] & [L^{56}] \\ [L^{61}] & [L^{62}] & [L^{63}] & [L^{64}] & [L^{65}] & [L^{66}] \end{bmatrix} \begin{bmatrix} \{F_1\} \\ \{H\} \\ \{F_2\} \\ \{\Theta\} \\ \{\Phi\} \\ \{\chi\} \end{bmatrix} = \begin{bmatrix} \{R_1\} \\ \{R_2\} \\ \{R_3\} \\ \{R_4\} \\ \{R_5\} \\ \{R_6\} \end{bmatrix} \tag{37}$$

where $[L_{mn}]$ and $[R_m]$ (m, n = 1, 2, 3, 4) matrices are written as:

$$L_{ij}^{11}=\int_{\Omega_e}\Upsilon_i\frac{d\Upsilon_j}{d\eta}d\Omega_e, L_{ij}^{12}=-\int_{\Omega_e}\Upsilon_i\Upsilon_j d\Omega_e, L_{ij}^{13}=L_{ij}^{14}=L_{ij}^{15}=L_{ij}^{21}=L_{ij}^{24}=L_{ij}^{25}=L_{ij}^{26}=0,$$

$$L_{ij}^{22}=-\frac{1}{\chi_1\chi_2}\int_{\Omega_e}\frac{d\Upsilon_i}{d\eta}\frac{d\Upsilon_j}{d\eta}d\Omega_e+\frac{1}{2}(1-\Gamma)\eta\int_{\Omega_e}\Upsilon_i\frac{d\Upsilon_j}{d\eta}d\Omega_e+\Gamma\int_{\Omega_e}\bar{F}_1\Upsilon_i\frac{d\Upsilon_j}{d\eta}d\Omega_e-\Gamma\int_{\Omega_e}\bar{H}\Upsilon_i\Upsilon_j d\Omega_e$$
$$-\frac{M^2}{\chi_2}\Gamma\int_{\Omega_e}\Upsilon_i\Upsilon_j d\Omega_e,$$
$$-\Gamma(1-\Gamma)\int_{\Omega_e}\Upsilon_i\frac{d\Upsilon_j}{d\Gamma}d\Omega_e,\ L_{ij}^{23}=2\lambda\Gamma\int_{\Omega_e}\Upsilon_i\Upsilon_j d\Omega_e,\ L_{ij}^{31}=L_{ij}^{34}=L_{ij}^{35}=L_{ij}^{36}=0,\ L_{ij}^{32}=-2\lambda\Gamma\int_{\Omega_e}\Upsilon_i\Upsilon_j d\Omega_e,$$

$$L_{ij}^{33}=-\frac{1}{\chi_1\chi_2}\int_{\Omega_e}\frac{d\Upsilon_i}{d\eta}\frac{d\Upsilon_j}{d\eta}d\Omega_e+\frac{1}{2}(1-\Gamma)\eta\int_{\Omega_e}\Upsilon_i\frac{d\Upsilon_j}{d\eta}d\Omega_e+\Gamma\int_{\Omega_e}\bar{F}_1\Upsilon_i\frac{d\Upsilon_j}{d\eta}d\Omega_e-\Gamma\int_{\Omega_e}\bar{H}\Upsilon_i\Upsilon_j d\Omega_e$$
$$-\Gamma(1-\Gamma)\int_{\Omega_e}\Upsilon_i\frac{d\Upsilon_j}{d\Gamma}d\Omega_e, L_{ij}^{41}=L_{ij}^{42}=L_{ij}^{43}=0,$$

$$L_{ij}^{44}=-\frac{\chi_3}{\chi_4}\int_{\Omega_e}\frac{d\Upsilon_i}{d\eta}\frac{d\Upsilon_j}{d\eta}d\Omega_e+\frac{Pr}{2}(1-\Gamma)\eta\int_{\Omega_e}\Upsilon_i\frac{d\Upsilon_j}{d\eta}d\Omega_e+P_r\zeta\int_{\Omega_e}\bar{F}_1\Upsilon_i\frac{d\Upsilon_j}{d\eta}d\Omega_e+P_rN_b\int_{\Omega_e}\bar{\Phi}'\Upsilon_i\frac{d\Upsilon_j}{d\eta}d\Omega_e$$
$$+P_rN_t\int_{\Omega_e}\bar{\Theta}'\Upsilon_i\frac{d\Upsilon_j}{d\eta}d\Omega_e-P_r\Gamma(1-\Gamma)\int_{\Omega_e}\Upsilon_i\frac{d\Upsilon_j}{d\Gamma}d\Omega_e, L_{ij}^{45}=L_{ij}^{46}=L_{ij}^{51}=L_{ij}^{52}=L_{ij}^{53}=L_{ij}^{56}=0,$$

$$L_{ij}^{54}=-\frac{N_t}{N_b}\int_{\Omega_e}\frac{d\Upsilon_i}{d\eta}\frac{d\Upsilon_j}{d\eta}d\Omega_e, L_{ij}^{55}=-\int_{\Omega_e}\frac{d\Upsilon_i}{d\eta}\frac{d\Upsilon_j}{d\eta}d\Omega_e+\frac{S_c}{2}(1-\Gamma)\eta\int_{\Omega_e}\Upsilon_i\frac{d\Upsilon_j}{d\eta}d\Omega_e+S_c\Gamma\int_{\Omega_e}\bar{F}_1\Upsilon_i\frac{d\Upsilon_j}{d\eta}d\Omega_e$$
$$-S_c\Gamma(1-\Gamma)\int_{\Omega_e}\Upsilon_i\frac{d\Upsilon_j}{d\Gamma}d\Omega_e, L_{ij}^{61}=L_{ij}^{62}=L_{ij}^{63}=L_{ij}^{64}=0,$$

$$L_{ij}^{65}=-P_e\delta_1\int_{\Omega_e}\frac{d\Upsilon_i}{d\eta}\frac{d\Upsilon_j}{d\eta}d\Omega_e, L_{ij}^{66}=-\int_{\Omega_e}\frac{d\Upsilon_i}{d\eta}\frac{d\Upsilon_j}{d\eta}d\Omega_e+\frac{S_b}{2}(1-\Gamma)\eta\int_{\Omega_e}\Upsilon_i\frac{d\Upsilon_j}{d\eta}d\Omega_e+S_b\Gamma\int_{\Omega_e}\bar{F}_1\Upsilon_i\frac{d\Upsilon_j}{d\eta}d\Omega_e$$
$$-P_e\int_{\Omega_e}\bar{\Phi}'\Upsilon_i\frac{d\Upsilon_j}{d\eta}d\Omega_e-P_e\int_{\Omega_e}\bar{\Phi}''\Upsilon_i d\Upsilon_j d\Omega_e-S_b\Gamma(1-\Gamma)\int_{\Omega_e}\Upsilon_i\frac{d\Upsilon_j}{d\zeta}d\Omega_e,$$

and

$$R_i^1=0,\ R_i^2=-\oint_{\Gamma_e}\Upsilon_i n_\eta\frac{\partial H}{\partial\eta}ds,\ R_i^3=-\oint_{\Gamma_e}\Upsilon_i n_\eta\frac{\partial F_2}{\partial\eta}ds,\ R_i^4=-\oint_{\Gamma_e}\Upsilon_i n_\eta\frac{\partial\Theta}{\partial\eta}ds,$$
$$R_i^5=-\oint_{\Gamma_e}\Upsilon_i n_\eta\frac{\partial\Phi}{\partial\eta}ds-\frac{N_t}{N_b}\oint_{\Gamma_e}\Upsilon_i n_\eta\frac{\partial\Theta}{\partial\eta}ds,\ R_i^6=-\oint_{\Gamma_e}\Upsilon_i n_\eta\frac{\partial\chi}{\partial\eta}ds. \tag{38}$$

where, $\bar{F}_1=\sum_{j=1}^{4}\bar{F}_{1j}\Upsilon_j, \bar{H}=\sum_{j=1}^{4}\bar{H}_j\Upsilon_j, \bar{F}_2=\sum_{j=1}^{4}\bar{F}_{2j}\Upsilon_j, \bar{\Theta}'=\sum_{j=1}^{4}\bar{\Theta}_j'\Upsilon_j$, and $\bar{\Phi}'=\sum_{j=1}^{4}\bar{\Phi}_j'\Upsilon_j$ supposed to be the known values. Compute 6 functions at each node. The obtained system of equations 61,206 are nonlinear after assembly, linearize using an iterative algorithm with the 10^{-5} precision necessary.

Results and discussion

We have demonstrated the importance of nanoparticle aggregation on the dynamics of suspensions containing microscopic particles spinning fluid susceptible to Lorentz and Coriolis forces, as well as gyrotactic microorganisms in this section. In every one of the figures, set of two curves are drawn for two specific cases: (1) $\Phi_{int}=1.0$ (non-aggregated nanoparticles) and (2) $\Phi_{int}\neq 1.0$ (aggregated nanoparticles). Further, the default values for other involved parameters and quantities are: $P_r=6.2$ (water-host fluid), $M=1.0, N_b=0.2, N_t=0.2, lambda=1.0$, $S_c=10.0, S_b=5.0, P_e=0.5, D=1.8, \delta_1=0.2, \Phi=0.01, \Phi_{max}=0.650$, and $R_a/R_p=3.34$. To verify the reliability and validity of Galerkin finite element approach, a grid independence study is performed. The problem input is distributed into various mesh density, and there is no more fluctuation is noted after 100×100, so we draw all the results on 100×100 grid size (see Table 3). To show that the current results are validate and reliable, a comparison with recently published studies are presented in Tables 3 and 4 in specific cases. The present outcomes are very close with the already published results, as evidenced. The friction factors along with primary and secondary directions $-F_1''(0)\&-F_2(0)$ in Table 4 against growing inputs of $\lambda=0.0, 1.0, 2.0, 5.0$ at $\Gamma=1.0$. The results achieved are in excellent agreement with those anlyzed by Ali et al.[45], and Wang[17]. Additionaly, in Table 5, the $-\Theta(0)$ inputs are acknowledged between Adnan et al.[52] and Bagh et al.[53], and present FEM results against growing inputs of $\lambda\&M$, and discovered that they are in accord. As a result, the numerical computations may be validated, and the Finite Element Computations produced using Matlab program have a high convergence rate.

The distribution of primary velocity $F_1'(\Gamma,\eta)$ and secondary velocity $F_2'(\Gamma,\eta)$ against exceeding inputs of magnetic (M) and rotating (λ) parameters are depicted in Figs. 3 and 4 respectively. Figure 3a,b portraits the $F_1'(\Gamma,\eta)$ and $F_2(\Gamma,\eta)$ for distinct inputs of magnetic field. The enhanced magnetic field caused to produce the resistive

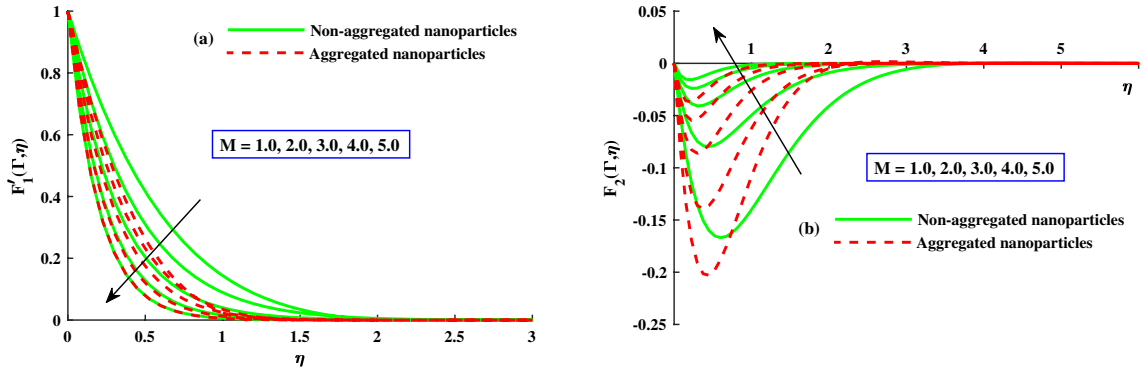

Figure 3. Variation of M on $F_1^{'}(\Gamma,\eta)$ in axial, and $F_2^{'}(\Gamma,\eta)$ in transverse.

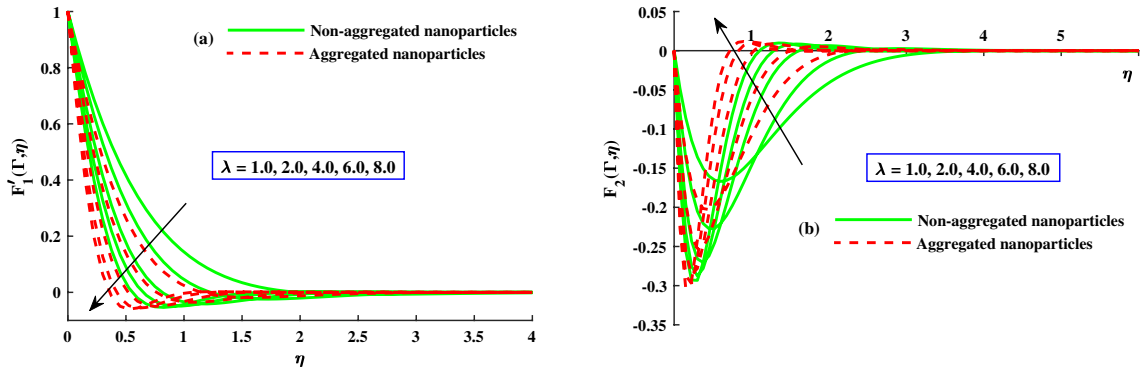

Figure 4. Variation of λ on $F_1^{'}(\Gamma,\eta)$ in axial, and $F_2^{'}(\Gamma,\eta)$ in transverse.

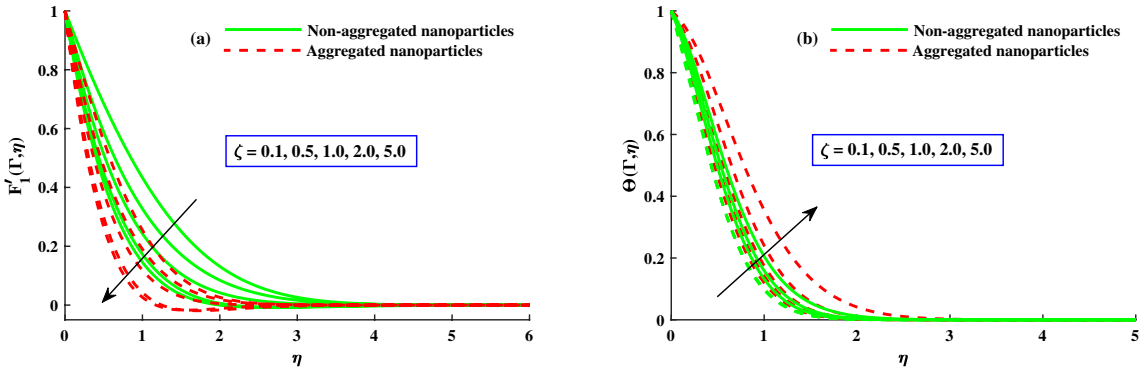

Figure 5. Variation of ζ on $F_1^{'}(\Gamma,\eta)$ in x-direction, and $\Theta(\Gamma,\eta)$.

force which called it Lorentz force and goes to recede of the primary velocity in Fig. 3b, whereas an inverse action is reported for secondary velocity in Fig. 3b. The impact of rotation parameter λ on axial velocity $F_1'(\Gamma,\eta)$ and transverse velocity $F_2(\Gamma,\eta)$ portrayed in Fig. 4a,b. It is observed that diminishing of axial velocity for exceeding inputs of *lambda* because of Coriolis force while an opposing action is claimed for transverse velocity in Fig. 4b. The role of ζ (unsteady parameter) on axial velocity and thermal profile is deliberated in Fig. 5a,b. The proceeding inputs of ζ the axial velocity curve reduced while thermal distribution improved. Hence, it clear that the time dependent parameter is play significance role in controlling the momentum and thermal boundary thickness. Further, from these figures, the model along with nanoparticles aggregation has a lower distribution of primary velocity $F_1'(\Gamma,\eta)$ and magnitude of secondary velocity $F_2'(\Gamma,\eta)$, whereas distribution of primary and secondary velocities are slightly greater than that considering the model of homogeneous (non-aggregated nanoparticles). Physically, the formation of nanoparticles aggregation caused to increase in the effective viscosity[54], and growing strength of viscosity is responsible to slow down the fluid velocity[55].

The distribution of friction factors $C_{f_x}Re_x{}^{1/2}$ (axial direction) and $C_{f_y}Re_x{}^{1/2}$ (transverse direction) against exceeding values of $\Gamma(0:0.2:1)$ and $M(1:1:5)$ parameters are depicted in Fig. 6a,b. Figure 6a demonstrates that for growing $\Gamma(0\rightarrow 1$, the axial friction factor $(C_{f_x}Re_x{}^{1/2})$ is enhanced steadily rise to a fixed rate, after which no noticeable change is noticed, but for increasing M, a remarkable diminution in axial friction factor $(C_{f_x}Re_x{}^{1/2})$

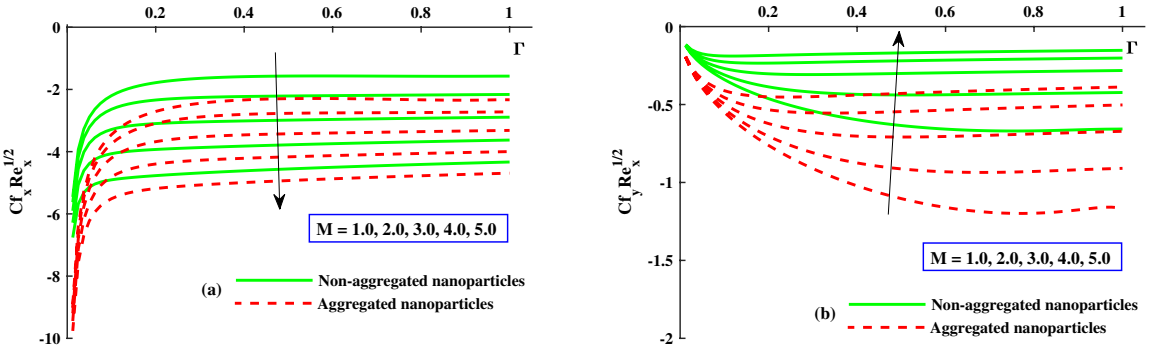

Figure 6. Variation of M on $Cf_x Re_x^{1/2}$ in x-direction, and $Cf_y Re_y^{1/2}$ in y-direction.

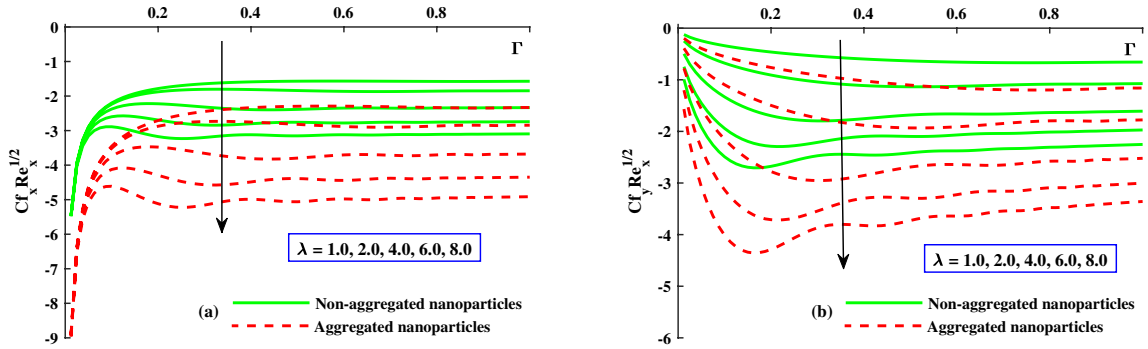

Figure 7. Variation of λ on $Cf_x Re_x^{1/2}$ in x-direction, and $Cf_y Re_y^{1/2}$ in y-direction.

is observed. For increasing $\Gamma(0 \rightarrow 1$, the transverse direction friction factor $(C_{f_y} Re_x{}^{1/2})$ magnitude is steadily lowered until it reaches a constant rate, after which no appreciable difference is noticed, as illustrated in Fig. 6b, while improving M, and see the significance difference near the surface. Figure 7a,b depicts that for growing $\Gamma(0 \rightarrow 1$, the axial skin friction $(C_{f_x} Re_x{}^{1/2})$ is progressively increased until it reaches a constant rate, afterwards which no substantial change is detected, whereas raising λ requires a large drop in axial direction skin factor $(C_{f_x} Re_x{}^{1/2})$ and transverse direction $(C_{f_y} Re_x{}^{1/2})$ is noticed. Furthermore, it is apparent from these graphs that the ranges of $(C_{f_x} Re_x{}^{1/2})$ and $(C_{f_y} Re_x{}^{1/2})$ for the model along with nanoparticles aggregation has a negatively lower distribution as compared to non-aggregated nanoparticles case.

The distribution of $\Theta(\Gamma, \eta)$ for different parameters is displayed in Figs. 8 and 9. The magnetic field parameter upgraded the $\Theta(\Gamma, \eta)$ (temperature distribution) which clearly seen in Fig. 8a. It is because of net force mentioned as Lorentz force around the internal electric force and external magnetic field control the temperature profile, which is showed in Fig. 8a, while the thermal boundary layer thickness is improved against increasinng λ as depict in Fig. 8b. Figure 9a,b displays that $\Theta(\Gamma, \eta)$ for distict inputs of thermophoresis (N_t) and Brownian motion (N_b) parameters. The exceeding strength of $N_t \& N_b$ caused to increased the distribution of temperature profile. The higher N_b, the quicker the erratic movement of nano particles in the flow domain, the better the thermal dispersion. Furthermore, the thermophorestic (Nt) effect drives micro entities to move from a hotter to a cooler location, boosting the $\Theta(\Gamma, \eta)$. Further, from these figures, the model without nanoparticles aggregation (homogeneous model) has a lower distribution of temperature $\Theta(\Gamma, \eta)$, whereas distribution of $\Theta(\Gamma, \eta)$ is slightly greater than that considering the model of nanoparticles aggregation. This result show that the nanoparticles aggregation has a positive effect on the nanofluid thermal conductivity[56,57]. The sketches of local Nusselt number $(Nu_x Re_x{}^{1/2})$ is depicted in Fig. 10a,b for $M(1:1:5) \& \lambda(1:2:8)$. For growing $M \& \lambda$, the distribution of $(Nu_x Re_x{}^{1/2})$ is decreased gradually. The nanoparticles aggregation model show a significant reduction in $(Nu_x Re_x{}^{1/2})$, whereas distribution of $Nu_x Re_x{}^{1/2}$ is slightly greater than that non-aggregated nanoparticles case.

The distribution of nanoparticles volume fraction $\Phi(\Gamma, \eta)$ and motile micoorganisms $\chi(\Gamma, \eta)$ against exceeding inputs of magnetic (M) and rotating (λ) parameters are depicted in Figs. 11 and 14 respectively. The tiny particles $(\Phi(\Gamma, \eta))$ and motile microorganisms $(\chi(\Gamma, \eta))$ profiles are upgraded for growing strength of magnetic and rotatory parameters as portraits in Figs. 11a,b and 14a,b. For exceeding values of ζ (time-dependent parameter) and Peclet number (P_e) parameters, the diminution of the thickness of the motile distribution is delineated in Figs. 12a,b. Hence, it clear that the time dependent parameter is play significance role in controlling the motile boundary thickness. Further, from these figures, the model along with nanoparticles aggregation has a greater distribution of concentration distributions, whereas distribution of nanoparticles and motile microorganisms primary are slightly greater than that considering the model of homogeneous (non-aggregated nanoparticles). The behavior of local Sherwood number $(Shr_x Re_x{}^{1/2})$ and motile microorganism density number $Re_x^{1/} N_x$ is

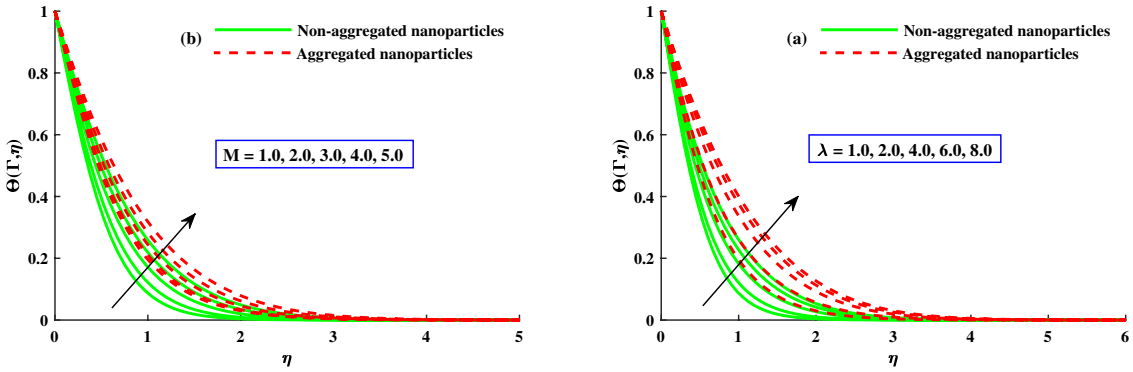

Figure 8. Variation of M and λ on $\Theta(\Gamma, \eta)$.

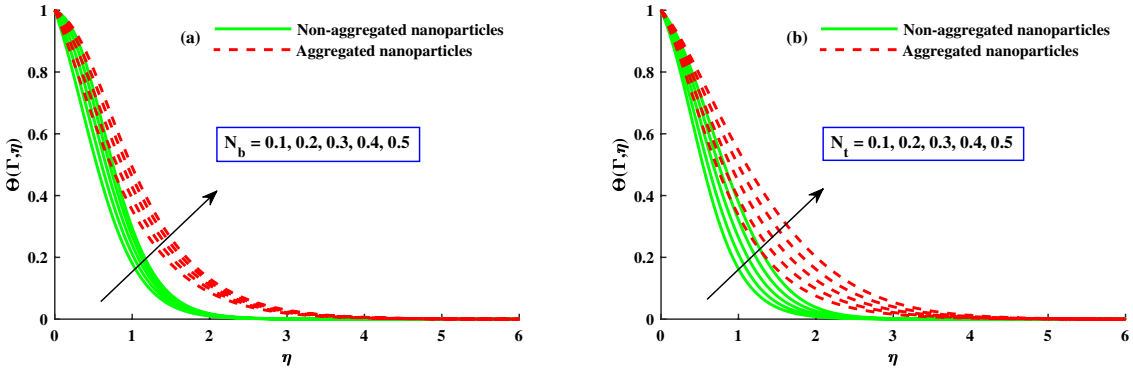

Figure 9. Variation of N_b and N_t on $\Theta(\Gamma, \eta)$.

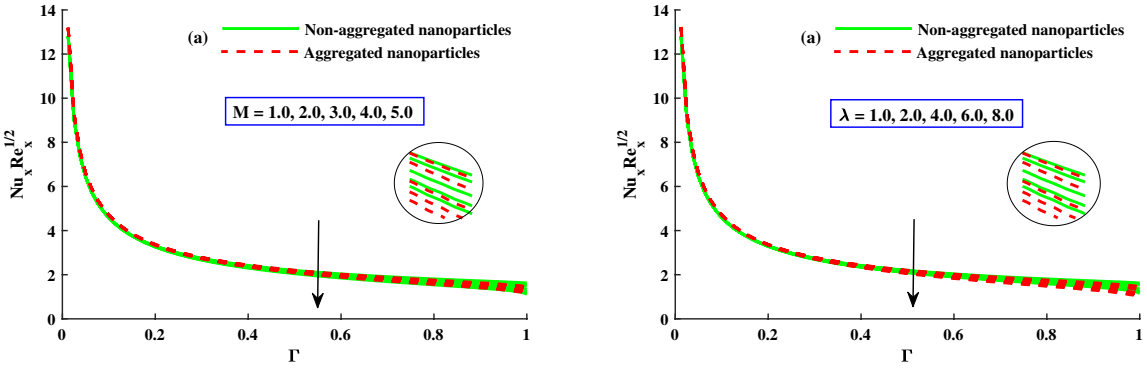

Figure 10. Variation of $Nu_x Re_x^1/2$ against M, and λ.

deliberated in Fig. 13a,b for enhancing strength of $M(0{:}1{:}4)\&\lambda(1{:}2{:}8)$, respectively. For enhancing $M\&\lambda$, the distribution of motile microorganism density number $Re_x^{1/} N_x$ and $(Shr_x Re_x{}^{1/2})$ is declined. and it is also witnessed that the non-aggregated case has larger $Shr_x Re_x{}^{1/2}$ and $Re_x^{1/} N_x$ than that of aggregated case (Fig. 14).

Conclusions

In this work, the Galerkin finite element study on the dynamics of rotating water based silver tiny particles subject to Coriolis, and Lorentz forces has been explored numerically along with swimming of motile organisms. The effective nanofluid viscosity and thermal conductivity has been studied by the authors for applying nanoparticles aggregation and homogeneous models. Depending on the outcomes of the analysis, it is reasonable to conclude that:

1. Exceeding values in the strength of Coriolis and Lorentz has a receding impact on the axial momentum and transverse momentum magnitude, and

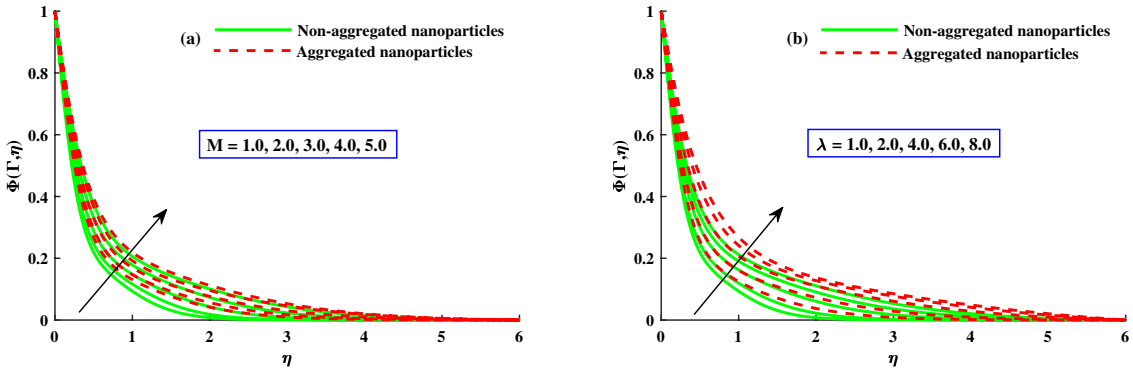

Figure 11. Variation of M and λ on $\Phi(\Gamma, \eta)$.

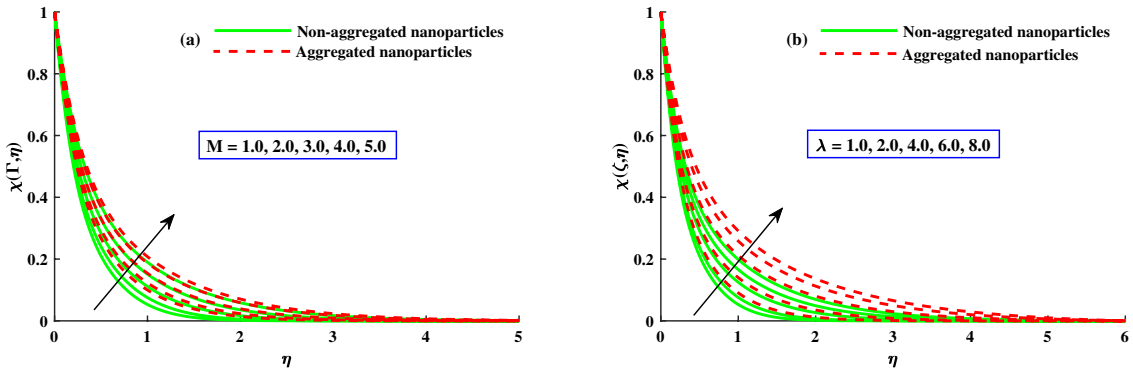

Figure 12. Variation of M and λ on $\chi(\Gamma, \eta)$.

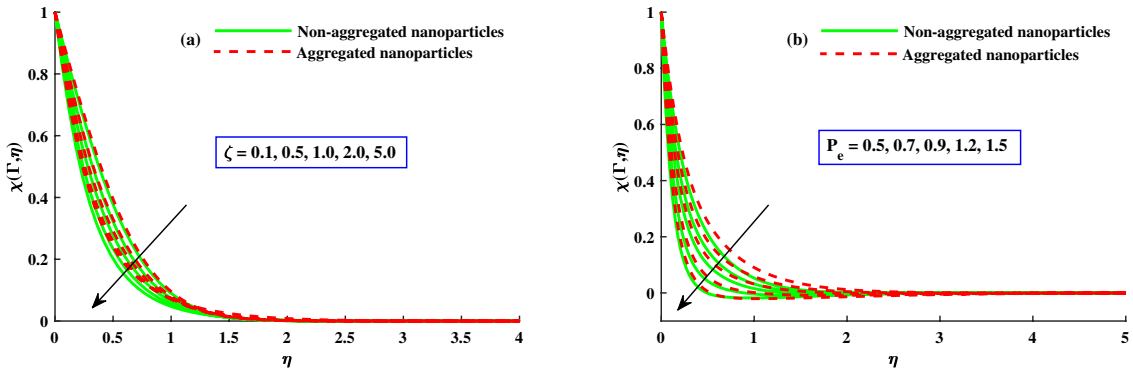

Figure 13. variation of Lb and Pe on $\chi(\Gamma, \eta)$ at $\zeta = 1$.

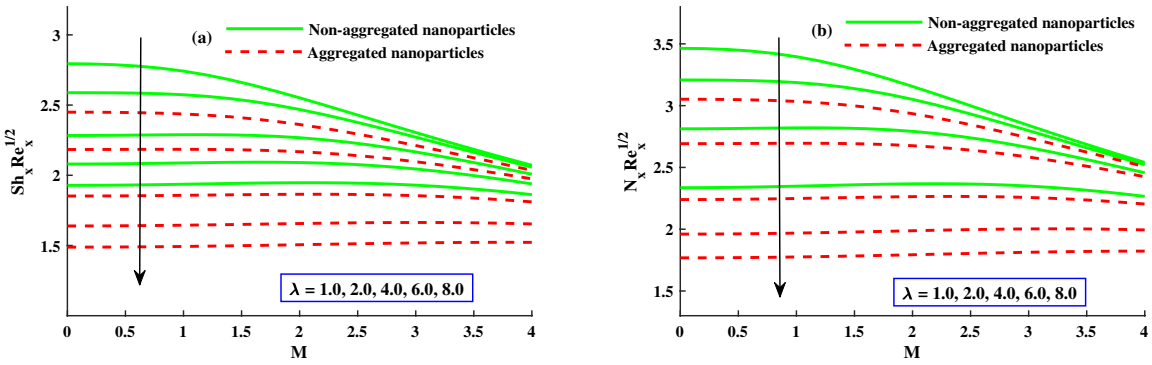

Figure 14. Variation of $Shr_x Re_x^1/2$ against N_b, N_t, M, and λ.

Grid size	$-F_1''(\zeta,0)$	$-F_2'(\zeta,0)$	$-\Theta'(\zeta,0)$	$-\Phi'(\zeta,0)$	$-\chi'(\zeta,0)$
20×20	2.2314	1.2404	0.4194	2.0326	2.7752
30×30	2.2172	1.2294	0.4367	1.9184	2.7376
50×50	2.2129	1.2168	0.4462	1.8603	2.6754
80×80	2.2122	1.2109	0.4463	1.8479	2.6461
100×100	2.2119	1.2094	0.4456	1.8451	2.6389
120×120	2.2118	1.2090	0.4454	1.8448	2.6386

Table 3. Analysis of grid independence for distinct grid sizes at $\zeta = 1.0$.

	Ali et al.[45]		Wang.[17]		Present	
λ	$-F_1''(0)$	$-F_2'(0)$	$-F_1''(0)$	$-F_2'(0)$	$-F_1''(0)$	$-F_2'(0)$
0.0	1.00000	0.00000	1.0000	0.0000	1.00000	0.00000
1.0	1.32501	0.83715	1.3250	0.8371	1.32501	0.83715
2.0	1.65232	1.28732	1.6523	1.2873	1.65232	1.28732
5.0	2.39026	2.15024	–	–	2.39026	2.15024

Table 4. Comparative of skin friction $-F_1^{'}(0)$ and $-F_2^{''}(0)$ for different inputs of λ at $zeta = 1$ while other factors are ignored.

	Adnan et al.[52]	Bagh et al.[53]	FEM (current outcomes)	
λ	$M = 0.0, Pr = 2.0$	$M = Pr = 2.0$	$M = 0.0, Pr = 2.0$	$M = Pr = 2.0$
0.0	0.911	0.6682	0.91107	0.66821
0.5	0.853	0.6627	0.85343	0.66268
1.0	0.770	0.6483	0.77028	0.64828
2.0	0.638	0.6030	0.63805	0.60303

Table 5. Comparative of $-\theta'(0)$ for different inputs of λ at $\xi = 1$ when others physical involved parameters are negligible.

- an enhancing influence on the profiles of thermal and concentrations boundary layers.
- Enhance the magnitude of $Cf_xRe_x^{1/2}$ (skin friction factor).
- a negative effects on $Nu_xRe_x{}^{1/2}$, $Shr_xRe_x{}^{1/2}$, and $N_xRe_x{}^{1/2}$.

A similar trend against higher values of rotation is reported by Oke et al.[21], and found that the increasing rotation caused to enhance the magnitude of skin friction coefficient, and mean while magnetic caused to decline in $Nu_xRe_x{}^{1/2}$.

2. Growing strength of Brownian motion, thermophoresis, and time-dependent parameters have an enhancing effect on the thermal distribution. The higher Bronian motion, the quicker the movement of nano particles in the flow domain, the better the thermal dispersion, and the thermophorestic effect drives micro entities to move from a hotter to a cooler location which caused to boosting the temperature[23,35].
3. Motile microorganism concentration diminishes against incremented Peclet number and time-dependent values.
4. Formation of nanoparticles aggregation has a declining impact on the axial and transverse velocities magnitude, but

- an exceeding impact on the profiles of temperature, tiny particles volume fraction, and motile microorganism.
- the nanoparticles aggregation case has lower the values of $C_{f_x}Re_x{}^{1/2}$ and $C_{f_y}Re_x{}^{1/2}$.
- the nanoparticles aggregation model show a significant reduction in $Nu_xRe_x{}^{1/2}$.
- the non-aggregated case has larger $Shr_xRe_x{}^{1/2}$ and $Re_x^{1/}N_x$ than that of aggregated case.

This work can be extended in the future for non-Newtonian based fluids susceptible to nanoparticles and other physical characteristics after a victorious simulated strife of parametric effects on fluid dynamics

Data availability

The data used to support the findings of this study are available from the corresponding author upon request.

Received: 21 June 2022; Accepted: 14 September 2022
Published online: 28 September 2022

References

1. Thumma, T., Bég, O. A. & Sheri, S. R. Finite element computation of magnetohydrodynamic nanofluid convection from an oscillating inclined plate with radiative flux, heat source and variable temperature effects. *Proc. Inst. Mech. Eng. Part N J. Nanomater. Nanoeng. Nanosyst.* **231**, 179–194 (2017).
2. Sheikholeslami, M. & Ebrahimpour, Z. Nanofluid performance in a solar LFR system involving turbulator applying numerical simulation. *Adv. Powder Technol.* **33**, 103669 (2022).
3. Shafiq, A. *et al.* Thermally enhanced Darcy-Forchheimer Casson-water/glycerine rotating nanofluid flow with uniform magnetic field. *Micromachines* **12**, 605 (2021).
4. Sheikholeslami, M. & Farshad, S. A. Nanoparticles transportation with turbulent regime through a solar collector with helical tapes. *Adv. Powder Technol.* **33**, 103510 (2022).
5. Sheikholeslami, M. Numerical investigation of solar system equipped with innovative turbulator and hybrid nanofluid. *Sol. Energy Mater. Sol. Cells* **243**, 111786 (2022).
6. Sheikholeslami, M. Analyzing melting process of paraffin through the heat storage with honeycomb configuration utilizing nanoparticles. *J. Energy Storage* **52**, 104954 (2022).
7. Shafiq, A., Çolak, A. B., Sindhu, T. N., Al-Mdallal, Q. M. & Abdeljawad, T. Estimation of unsteady hydromagnetic Williamson fluid flow in a radiative surface through numerical and artificial neural network modeling. *Sci. Rep.* **11**, 1–21 (2021).
8. Sridhar, V., Ramesh, K., Gnaneswara Reddy, M., Azese, M. N. & Abdelsalam, S. I. On the entropy optimization of hemodynamic peristaltic pumping of a nanofluid with geometry effects. *Waves Random Complex Media* **5**, 1–21 (2022).
9. Abdelsalam, S. I., Mekheimer, K. S. & Zaher, A. Dynamism of a hybrid Casson nanofluid with laser radiation and chemical reaction through sinusoidal channels. *Waves Random Complex Media* **22**, 1–22 (2022).
10. Bhatti, M. M., Bég, O. A. & Abdelsalam, S. I. Computational framework of magnetized MGO-NI/water-based stagnation nanoflow past an elastic stretching surface: Application in solar energy coatings. *Nanomaterials* **12**, 1049 (2022).
11. Alsharif, A., Abdellateef, A., Elmaboud, Y. & Abdelsalam, S. Performance enhancement of a dc-operated micropump with electroosmosis in a hybrid nanofluid: Fractional cattaneo heat flux problem. *Appl. Math. Mech.* **43**, 931–944 (2022).
12. Thumma, T., Mishra, S., Abbas, M. A., Bhatti, M. M. & Abdelsalam, S. I. Three-dimensional nanofluid stirring with non-uniform heat source/sink through an elongated sheet. *Appl. Math. Comput.* **421**, 126927 (2022).
13. Sheikholeslami, M. & Ebrahimpour, Z. Thermal improvement of linear fresnel solar system utilizing al2o3-water nanofluid and multi-way twisted tape. *Int. J. Therm. Sci.* **176**, 107505 (2022).
14. Sheikholeslami, M., Said, Z. & Jafaryar, M. Hydrothermal analysis for a parabolic solar unit with wavy absorber pipe and nanofluid. *Renew. Energy* **188**, 922–932 (2022).
15. Abdelsalam, S. I. *et al.* Couple stress fluid flow in a rotating channel with peristalsis. *J. Hydrodyn.* **30**, 307–316 (2018).
16. Ali, B., Naqvi, R. A., Mariam, A., Ali, L. & Aldossary, O. M. Finite element study for magnetohydrodynamic (MHD) tangent hyperbolic nanofluid flow over a faster/slower stretching wedge with activation energy. *Mathematics* **9**, 25 (2021).
17. Wang, C. Stretching a surface in a rotating fluid. *Z. Angew. Math. Phys.* **39**, 177–185 (1988).
18. Takhar, H. S., Chamkha, A. J. & Nath, G. Flow and heat transfer on a stretching surface in a rotating fluid with a magnetic field. *Int. J. Therm. Sci.* **42**, 23–31 (2003).
19. Awan, A. U., Ahammad, N. A., Majeed, S., Gamaoun, F. & Ali, B. Significance of hybrid nanoparticles, lorentz and coriolis forces on the dynamics of water based flow. *Int. Commun. Heat Mass Transfer* **135**, 106084 (2022).
20. Lou, Q. *et al.* Micropolar dusty fluid: Coriolis force effects on dynamics of MHD rotating fluid when Lorentz force is significant. *Mathematics* **10**, 2630 (2022).
21. Oke, A. S., Mutuku, W. N., Kimathi, M. & Animasaun, I. L. Coriolis effects on MHD newtonian flow over a rotating non-uniform surface. *Proc. Inst. Mech. Eng. C J. Mech. Eng. Sci.* **235**, 3875–3887 (2021).
22. Chu, Y.-M. *et al.* Nonlinear radiative bioconvection flow of Maxwell nanofluid configured by bidirectional oscillatory moving surface with heat generation phenomenon. *Phys. Scr.* **95**, 105007 (2020).
23. Rao, M. V. S., Gangadhar, K., Chamkha, A. J. & Surekha, P. Bioconvection in a convectional nanofluid flow containing gyrotactic microorganisms over an isothermal vertical cone embedded in a porous surface with chemical reactive species. *Arab. J. Sci. Eng.* **46**, 2493–2503 (2021).
24. Awais, M. *et al.* Effects of variable transport properties on heat and mass transfer in MHD bioconvective nanofluid rheology with gyrotactic microorganisms: Numerical approach. *Coatings* **11**, 231 (2021).
25. Abdelmalek, Z., Ullah Khan, S., Waqas, H., A Nabwey, H. & Tlili, I. Utilization of second order slip, activation energy and viscous dissipation consequences in thermally developed flow of third grade nanofluid with gyrotactic microorganisms. *Symmetry* **12**, 309 (2020).
26. Shafiq, A., Rasool, G., Khalique, C. M. & Aslam, S. Second grade bioconvective nanofluid flow with buoyancy effect and chemical reaction. *Symmetry* **12**, 621 (2020).
27. Murshed, S., Leong, K. & Yang, C. Enhanced thermal conductivity of TiO2-water based nanofluids. *Int. J. Therm. Sci.* **44**, 367–373 (2005).
28. Prasher, R., Phelan, P. E. & Bhattacharya, P. Effect of aggregation kinetics on the thermal conductivity of nanoscale colloidal solutions (nanofluid). *Nano Lett.* **6**, 1529–1534 (2006).
29. Daungthongsuk, W. & Wongwises, S. A critical review of convective heat transfer of nanofluids. *Renew. Sustain. Energy Rev.* **11**, 797–817 (2007).
30. Liu, M.-S., Lin, M.C.-C., Tsai, C. & Wang, C.-C. Enhancement of thermal conductivity with cu for nanofluids using chemical reduction method. *Int. J. Heat Mass Transf.* **49**, 3028–3033 (2006).
31. Zhu, H. T., Zhang, C. Y., Tang, Y. M. & Wang, J. X. Novel synthesis and thermal conductivity of CuO nanofluid. *J. Phys. Chem. C* **111**, 1646–1650 (2007).
32. Wang, B.-X., Zhou, L.-P. & Peng, X.-F. A fractal model for predicting the effective thermal conductivity of liquid with suspension of nanoparticles. *Int. J. Heat Mass Transf.* **46**, 2665–2672 (2003).
33. Hamilton, R. L. & Crosser, O. Thermal conductivity of heterogeneous two-component systems. *Ind. Eng. Chem. Fundam.* **1**, 187–191 (1962).
34. Khan, S. A., Nie, Y. & Ali, B. Multiple slip effects on magnetohydrodynamic axisymmetric buoyant nanofluid flow above a stretching sheet with radiation and chemical reaction. *Symmetry* **11**, 1171 (2019).
35. Ali, B., Hussain, S., Nie, Y., Khan, S. A. & Naqvi, S. I. R. Finite element simulation of bioconvection Falkner–Skan flow of a Maxwell nanofluid fluid along with activation energy over a wedge. *Phys. Scr.* **95**, 095214 (2020).
36. Ali, B., Hussain, S., Nie, Y., Rehman, A. U. & Khalid, M. Buoyancy effects on Falknerskan flow of a Maxwell nanofluid fluid with activation energy past a wedge: Finite element approach. *Chin. J. Phys.* **68**, 368–380 (2020).
37. Sheri, S. R. & Thumma, T. Heat and mass transfer effects on natural convection flow in the presence of volume fraction for copper-water nanofluid. *J. Nanofluids* **5**, 220–230 (2016).

38. Sheri, S. R. & Thumma, T. Double diffusive magnetohydrodynamic free convective flow of nanofluids past an inclined porous plate employing tiwari and das model: Fem. *J. Nanofluids* **5**, 802–816 (2016).
39. Ali, B., Rasool, G., Hussain, S., Baleanu, D. & Bano, S. Finite element study of magnetohydrodynamics (MHD) and activation energy in Darcy-Forchheimer rotating flow of Casson carreau nanofluid. *Processes* **8**, 1185 (2020).
40. Abbas, Z., Javed, T., Sajid, M. & Ali, N. Unsteady MHD flow and heat transfer on a stretching sheet in a rotating fluid. *J. Taiwan Inst. Chem. Eng.* **41**, 644–650 (2010).
41. Babu, M. J. & Sandeep, N. 3d MHD slip flow of a nanofluid over a slendering stretching sheet with thermophoresis and brownian motion effects. *J. Mol. Liq.* **222**, 1003–1009 (2016).
42. Hayat, T., Muhammad, T., Shehzad, S. & Alsaedi, A. Three dimensional rotating flow of Maxwell nanofluid. *J. Mol. Liq.* **229**, 495–500 (2017).
43. Ali, B., Hussain, S., Nie, Y., Hussein, A. K. & Habib, D. Finite element investigation of dufour and soret impacts on mhd rotating flow of oldroyd-b nanofluid over a stretching sheet with double diffusion cattaneo christov heat flux model. *Powder Technol.* **377**, 439–452 (2021).
44. Rosali, H., Ishak, A., Nazar, R. & Pop, I. Rotating flow over an exponentially shrinking sheet with suction. *J. Mol. Liq.* **211**, 965–969 (2015).
45. Ali, B., Naqvi, R. A., Ali, L., Abdal, S. & Hussain, S. A comparative description on time-dependent rotating magnetic transport of a water base liquid H_2 O with hybrid nano-materials Al_2 O_3 − Cu and Al_2 O_3 − TiO_2 over an extending sheet using buongiorno model: Finite element approach. *Chin. J. Phys.* **20**, 20 (2021).
46. Mahanthesh, B. & Thriveni, K. Nanoparticle aggregation effects on radiative heat transport of nanoliquid over a vertical cylinder with sensitivity analysis. *Appl. Math. Mech.* **42**, 331–346 (2021).
47. Reddy, G. J., Raju, R. S. & Rao, J. A. Influence of viscous dissipation on unsteady MHD natural convective flow of Casson fluid over an oscillating vertical plate via fem. *Ain Shams Eng. J.* **9**, 1907–1915 (2018).
48. Reddy, J. N. *Solutions Manual for an Introduction to the Finite Element Method* (McGraw-Hill, 1993).
49. Jyothi, K., Reddy, P. S. & Reddy, M. S. Carreau nanofluid heat and mass transfer flow through wedge with slip conditions and nonlinear thermal radiation. *J. Braz. Soc. Mech. Sci. Eng.* **41**, 415 (2019).
50. Ali, B., Pattnaik, P., Naqvi, R. A., Waqas, H. & Hussain, S. Brownian motion and thermophoresis effects on bioconvection of rotating Maxwell nanofluid over a riga plate with Arrhenius activation energy and cattaneo-christov heat flux theory. *Therm. Sci. Eng. Progress* **20**, 100863 (2021).
51. Ali, B., Yu, X., Sadiq, M. T., Rehman, A. U. & Ali, L. A finite element simulation of the active and passive controls of the MHD effect on an axisymmetric nanofluid flow with thermo-diffusion over a radially stretched sheet. *Processes* **8**, 207 (2020).
52. Butt, A. S., Ali, A. & Mehmood, A. Study of flow and heat transfer on a stretching surface in a rotating casson fluid. *Proc. Natl. Acad. Sci. India Sect. A* **85**, 421–426 (2015).
53. Ali, B., Naqvi, R. A., Hussain, D., Aldossary, O. M. & Hussain, S. Magnetic rotating flow of a hybrid nano-materials Ag − MoS_2 and Go − MoS_2 in C_2 H_6 O_2 − H_2 O hybrid base fluid over an extending surface involving activation energy: Fe simulation. *Mathematics* **8**, 1730 (2020).
54. Gharagozloo, P. E. & Goodson, K. E. Temperature-dependent aggregation and diffusion in nanofluids. *Int. J. Heat Mass Transf.* **54**, 797–806 (2011).
55. Ali, B., Nie, Y., Hussain, S., Habib, D. & Abdal, S. Insight into the dynamics of fluid conveying tiny particles over a rotating surface subject to Cattaneo–Christov heat transfer, coriolis force, and arrhenius activation energy. *Comput. Math. Appl.* **93**, 130–143 (2021).
56. Wei, W. *et al.* Fractal analysis of the effect of particle aggregation distribution on thermal conductivity of nanofluids. *Phys. Lett. A* **380**, 2953–2956 (2016).
57. Chen, H., Witharana, S., Jin, Y., Kim, C. & Ding, Y. Predicting thermal conductivity of liquid suspensions of nanoparticles (nanofluids) based on rheology. *Particuology* **7**, 151–157 (2009).

Acknowledgements

The 3rd author Rifaqat Ali extends his appreciation to Deanship of Scientific Research at King Khalid University, Saudi Arabia for funding this work through large Groups Project under Grant number R.G.P. 2/51/43. The researchers would like to thank the Deanship of Scientific Research, Qassim University for funding the publication of this project.

Author contributions

Conceptualization; B.A. and I.S. Methodology; F.J. and R.A. Writing—original draft preparation; I.S. and B.A. Data curation; J.A. Formal analysis; F.J. Funding acquisition; J.A. Investigation; H.A.E.-W.K. Resources; B.A. Software; R.A. Validation; J.A. Visualization; H.A.E.-W.K. Writing—review and editing; F.J., J.A. and H.A.E.-W.K. Supervision; I.S. All authors have read and agreed to the published version of the manuscript.

Competing interests

The authors declare no competing interests.

Additional information

Correspondence and requests for materials should be addressed to I.S., F.J. or H.A.E.-W.K.